Applied Thermal Engineering, Volume 186, March 2021, Article number 116299
DOI:10.1016/j.applthermaleng.2020.116299

Effect of Mist/Steam Uniformity on Heat Transfer Characteristics in Unconfined Jet Impingement

Hamad M. Alhajeri [1], Abdulrahman Almutairi [1], Abdulrahman Alenezia [1], Abdelaziz A.A. Gamil [2], M. H. Al-Hajeri [1]

[1] College of Technological Studies, PAAET, Shuwaikh, Kuwait

[2] Power Engineering Centre, Cranfield University, Bedford, UK

ABSTRACT

This paper presents the numerical investigations of the injection of mist into an unconfined cooling steam jet to analyze the effects on the corresponding heat transfer characteristics. The infusion of mist into an confined cooling steam jet demonstrates a remarkable improvement in the heat transfer specifications as described in numerous previous studies. Therefore, the current research contributes to the knowledge by focusing on the uniformity configurations of the injected second phase to the unconfined regions and the influence of the surrounding environment on the mist injected. Several variables govern the physical model of the mist concentration and jet to plate distance, which is included in three-dimensional incompressible Navier-Stokes flow with the discrete phase model for the multiphase flow regime. The simulation was conducted over a range of common working Reynolds numbers. The results show that controlling the uniformity of the injected mist will redefine the cooling characteristics. The accumulated mist near the edge leads to the heat transfer enhancement at H/D = 2, 4, and 6. The surrounding environment had a significant influence on the droplet behavior at H/D = 8, thus causing a heat transfer reduction of 8%. The droplet Stock number can determine the droplet performance on the target wall and introducing mist generates a third heat transfer peak that results in an average increase of 38% for 1% mist.

Keywords: Heat transfer; Unconfined jet impingement; Mist-steam mixture; Droplet uniformity

1. Introduction

Impinging jets are characterized by high convective heat transfer specifications compared with other internal and external cooling techniques. Impinging jets are used in several industrial applications which need to transfer heat with high rates such as electronic, metal annealing, glass tempering, drying, and aircraft cooling systems [1]. Further advancements in the functionality of impinging jets are believed to be modifications to the jet configurations, target wall shape, confinement of the region, jet fluid type, and flow regime. However, other approaches are also compared to the jet impingement technique in terms of heat transfer efficiency.

A remarkable number of researchers have investigated the jet impingement features in confined conditions [2–10]. Previous research has highlighted attempts to increase the heat transfer of confined synthetic air jets using ducting plates with the distance from the jet exit assisting to draw cold air in with the jet flow [11]. Heat transfer enhancement of the jet impinging a cylindrical surface in a quadrilateral confined control volume [12] and observation of the heat transfer enhancement in minimal nozzle-to-plate distances both in single phase and two-phase mist impinging jets in a confined area [13]. Tan et al. studied the heat transfer details of the jet impingement technique in semi-confined regions [14].

The effect of the jet shapes and jet fluid has also attracted interest for heat transfer enhancement. For instance, to recognize that a circular jet can be outperformed by an assisting coaxial jet [15] and investigate of different jet cross-sections [16]. The results of the later study show that for certain jet shapes, specific values for mist addition could produce more sustainable heat exchange performance.

In the literature, the shape of the surface to be cooled is considered an important research issue. As a common approach, a ribbed target surface has been considered with a semi-confined jet with different rib shapes, jet to target distances (H/D), and Reynolds (Re) numbers [14]. The effect of mist/air jet impingement on a concave wall, which was roughened by a convex rib, was investigated by Bian et al. [17]. Furthermore, the curvature of the surface has been the focus of previous experiments. For example, the local enhancement of the heat transfer coefficient is reported around a cylinder. In a confined space, flow acceleration and high circulation is suppressed [12] and the curvature effects of the target surface in convex and concave configurations on heat transfer in the case of confined jets was investigated [18].

Water droplets addition in an air confined jet is shown to cause remarkable increase in the intensity of heat transfer near the jet stagnation point. Based on the single phase air impact jet, a substantial increase in the heat transfer area is apparent compared to the single phase air only jet case [19–22]. In addition, the effects of the mixture of mist/steam on the heat transfer quality using confined jets are presented [23,24]. The enhancement of heat transfer process using the mist/steam approach has a higher specific heat capacity at constant pressure compared to the steam. The mechanism of heat removal from the walls using the mist/steam technique can be described by the following steps. Considerable heat is absorbed due to the latent-heat evaporation, which works as a heat sink, and it causes a reduction in the bulk-temperature and increment to the temperature gradient adjacent to the walls. The increment in the temperature gradient increases the amount of conductive heat transfer from the walls. It also speeds up the evaporation process of the liquid particles. The transportation of the energy from the metal to the main flow was increased by the propulsive momentum which was emphasized by the fluid droplet evaporation. Finally, the motion of the steam particles improves the flow mixing characteristics as a result of particles injection and evaporation, resulting in an increase in the heat transfer process.

Based on the above review, the majority of previous studies have focused on the mist/steam impinging jet for a confined jet only and to the best of our knowledge, there has been no prior publication regarding the effects of mist addition on heat transfer of an unconfined steam jet. Furthermore, a difference exists between the thermal performance of the jet in a confined condition to that in an unconfined condition; in the case of fixed pumping power, the heat exchange rate of the unconfined jet remains an

area for further research, compared to that of the confined jet. This study aims to investigate the effect of mist/steam on an unconfined jet impingement. The water droplets distributions will be performed on a uniform and non-uniform (concentrated) distribution at the jet edge. The H/D, mist fractions, particle size behaviors, and various Re numbers will be examined.

2. Physical Model and Numerical Methods

The unsteady three-dimensional incompressible Navier-Stokes equations were solved using the finite volume method. The SIMPLEC method was employed for pressure-velocity couplings. The second-order upwind scheme was used to approximate the momentum equations and turbulent fluxes for the inviscid fluxes. The PRESTO interpolation was utilized for pressure while the cell-based Green-Gauss theorem was used to approximate the gradients. The discrete phase model (DPM) is considered an adequate method to simulate the water droplets because the mist volume fraction is less than 10% of the main flow. The DPM uses the Lagrangian approach to calculate the droplet trajectories of the dispersed phase by tracking each droplet from its origin. All simulations were performed using the ANSYS FLUENT software.

2.1 Governing Equations

The partial differential equations used in the CFD simulations which govern the fluid motion (Navier-Stokes equations) are:

Conservation of mass:

$$\frac{\partial \rho}{\partial t} + \nabla (\rho . \vec{u}) = 0 \tag{1}$$

Momentum:

$$\frac{\partial}{\partial t}(\rho.\vec{u}) + \nabla.(\rho.\vec{u}.\vec{u}) = -\nabla p + \nabla.\vec{\tau} + S_M \tag{2}$$

Energy:

$$\frac{\partial(\rho I_{total})}{\partial t} - \frac{\partial p}{\partial t} + \nabla.(\rho \vec{u} I_{total}) = \nabla.(k \nabla T) + \nabla.(\vec{u}.\vec{\tau}) + \vec{u}.S_M + S_E . \tag{3}$$

Discrete Phase

Here, we simulate the evolution of the particles in the Lagrangian frame in the discrete phase. For the discrete phase, the movement of the fluid particles is modeled in the Lagrangian frame. The transport equations are also solved simultaneously to uncover the dynamics of the continuous phase. Conversely, the mist is modeled as fluid particles

with spherical shapes. These particles spread as Lagrangian objects in the continuous phase. The movement of the small fluid particles are modeled using the following equation:

$$du_p / dt = F_D(u - u_p) + \frac{g_x(\rho_p - \rho)}{\rho_p} + F_{vm} + F_x . \quad (4)$$

In the above equation, the drag and gravity forces per unit mass are represented using the terms $F_D(u-u_p)$ and $g_x(\rho_p- \rho)/\rho_p$, respectively, while the virtual mass forces are calculated in Eq. 5 using the F_{vm} term. Moreover, the term (F_x) is added to Eq. 5 to calculate the additional forces in the model such as pressure-gradients, and thermophoretic and non-fixed reference frames. The acceleration due to gravity is shown by g_x, while the fluid density and velocity are ρ and u. Similarly, the particle density and velocity are represented by ρ_p and u_p, respectively.

The particle temperature is a variable of the interaction of the sensible heat variation inside the particles with both convective and latent heat transfer between the continuous phase and fluid particle. The governing equation for energy is the rate of change of temperature of the particles and, therefore, the energy-balance equation provides the variation of the particle temperature per unit time as

$$\frac{d(m_p.T_p.C_w)}{dt} = A_p k Nu_p (T - T_p) + \frac{dm_p}{dt} I_{fg} \quad . \quad (5)$$

In the above balance equation, the surface area and mass of the particles are represented by m_p and A_P , respectively. T is the fluid temperature and T_p represents the small droplets temperature. The amount of evaporation per unit time is denoted by dm_p/d_t, while I_{fg} is the latent heat. The Nusselt number Nu_p can be acquired empirically [25] as

$$Nu_p = 2 + 0.6 \mathrm{Re}_p^{0.5} (\mu C_p / k)^{0.33} \quad (6)$$

where, Nu_p and Re_p represent the Nu and Re numbers of the particle. The mass-transfer regulating agent is the gradient diffusion which encompasses the particle vapor flow into the fluid gas phase. This quantity corresponds to the gradient of the vapor concentration distribution between the particles and the main gas and it can be expressed as

$$\frac{dm_p}{dt} = -A_p k Nu_p (T - T_p) / I_{fg} . \quad (7)$$

Furthermore, if the particle temperature is less than the boiling point, the mass transfer can be calculated as

$$\frac{dm_p}{dt} = A_p \rho_v D_v \, Sh(\frac{M_v}{M}) \log[\frac{1-f_p}{1-f}] \tag{8}$$

In the above equation, D_V and ρ_V represent the vapor phase diffusive rate and density value, *Sh* is the Sherwood number, M_V and M denote the weight of the vapor and the mixture within the continuous phase at a molecular scale, and f and f_P represent the gas and particles molar fractions. *Sh* is calculated as

$$Sh = 2 + 0.6\,\mathrm{Re}_p^{0.5}\,(\mathrm{Pr})^{0.3} \tag{9}$$

2.2 Computational Domain and Boundary Conditions

The model of the fluid domain is illustrated in Figure 1. The jet flux from the nozzle with diameter D moves into a cylindrical domain of fluid with a diameter of 24D and a height H. The impinging of the jet occurs at the heated wall at H/D = 2, 4, 6, and 8 from the nozzle exit. The Re number is calculated using the nozzle diameter D and the bulk nozzle exit velocity U. The simulated region is a section of pipe with length 2D and diameter D with the domain upstream of the exit of the nozzle providing the applicability of the inflow boundary condition. The diameter of the cylindrical fluid domain is illustrated in Figure 1. Please note that the diameter includes the buffer region. A grid independence study was conducted to ensure that the chosen mesh size had little influence on the results obtained.

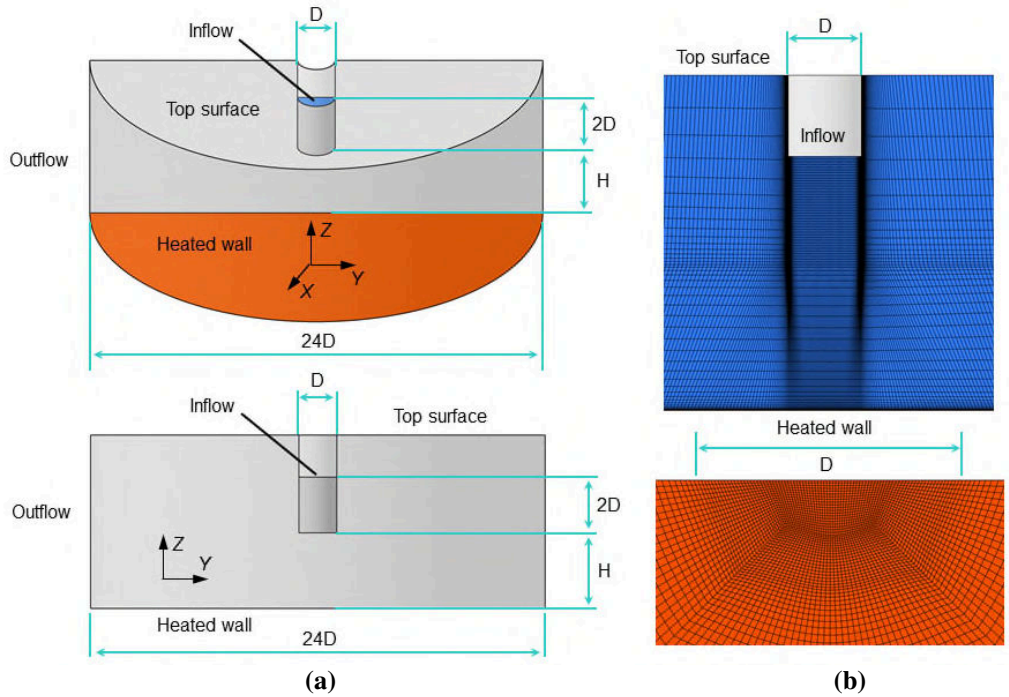

Figure 1 (a) Computational domain; (b) Grid topology

The environment settings and boundary conditions have been considered as listed in Table 1. The flow is a saturated vapor. The inlet flow temperature and ambient temperature are equal, and the saturation temperature is 105 °C. Such conditions are specially chosen for the droplets to start evaporating only in the thin wall-adjacent area, where the temperature is greater than the saturation temperature of 105 °C. The inlet Re number range is from 15,000 to 45,000.

Table 1 Simulation parameters

Re	D	μ_v	ρ_v	T_{inlet}	λ	T_{wall}
15,000–45,000	0.0135 m	$1.34e^{-05}$ $kg{\cdot}m^{-1}s^{-1}$	0.55 $kg{\cdot}m^{-3}$	105 °C	0.0261 $W{\cdot}m^{-1}K^{-1}$	150 °C

The Re number is calculated as follows:

$$Re = U_{ref} D / \mu \tag{10}$$

where, U_{ref} is the mass flow average inlet velocity, D is the inlet pipe diameter, and μ and ρ are the vapor viscosity and density, respectively. The Nusselt number can be calculated from Eq. 11:

$$Nu = Q D / (\lambda (T_{inlet} - T_{wall})) \tag{11}$$

where, Q is the wall heat flux, T_{inlet} is the inlet temperature, λ is the thermal conductivity, and T_{wall} is the heated wall temperature.

3. Result and Discussion

3.1 Numerical Method Validation

Unconfined jet impingement modeling strongly depends on the flow exit and environment boundary conditions. The experimental test geometry used by Katti and Prabhu [26] is adopted as a reference in this study. First, the cooling fluid is considered to be air only. The effects of the water droplets addition will then be investigated. This geometry has been widely used in numerous experimental and numerical studies. Several turbulence models are used for validation, the shear stress transport k-ω (SST), shear stress transport k- ω (SST) transition, and K-ε RNG. As described by Hofmann et al. [27], among all other turbulence models, the SST k- ω model can assess the laminar to turbulent transition phenomenon for modeling high Re number jet impingement and the ability to predict the heat transfer accurately. The solution was initialized using the standard initialization by inlet conditions with convergence criteria of 10^{-6} for energy and continuity equations, and 10^{-5} for the other equations.

Figure 2a shows the local Nu number along the heated wall for computational and experimental results [5,26,27]. A circular free jet shape is modeled at z/D = 6 and Re = 23,000, the inlet flow is considered as a fully developed flow at the heated wall,

and the thermal flow was fixed at Q = 7.54 kW·m^{-2}. The local Nu number along the target wall is calculated for three turbulence models and compared with the experimental data available in the literature. The result shows that the local Nu number of the model k- ε RNG is underestimated while the local Nu number of the model SST k- ω is slightly overestimated at the stagnation point. However, the local Nu number profiles of SST k-ω show good consistency with the experimental results where, at the stagnation point the deviation is limited to 3.3%. Therefore, with this justification, and with reference to the evidence presented by Hofmann et al. [28], the K- ω SST turbulence model is selected for all calculations in this study.

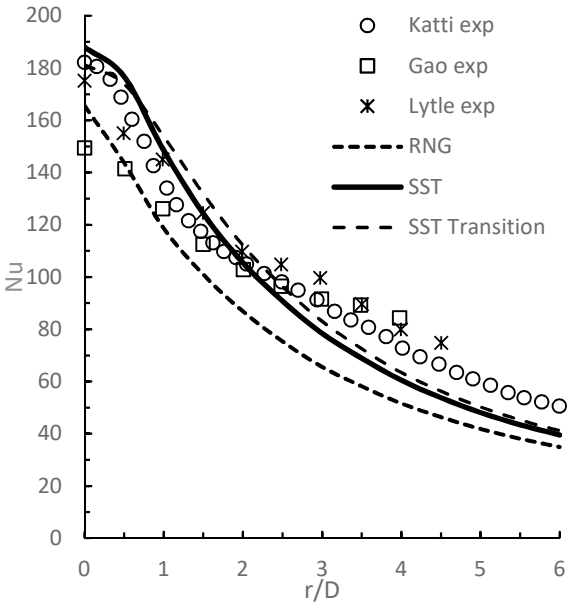

Figure 2 Local Nusselt number distribution comparison using different computational and experimental studies for single phase steam flow

3.2 Effects of Droplet Diameter on Particle Behavior

Several studies have been conducted on types of droplet impacts [29,30], which consider the Weber (We) number, wall temperature, presence or absence of the liquid film on the wall, impingement angle of the drops, and the droplet contact angle. The We number is defined by the following formula:

$$\mathrm{We} = \rho d V_{\mathrm{inlet}}^2/\sigma \qquad 12$$

where, ρ is the droplet density, d is the droplet diameter, V_{inlet} is the inlet velocity, and σ is the droplet contact angle.

Table 2 presents the values of the We and Stokes (Sk) numbers, which are considered in this study. The Sk number is a dimensionless parameter responsible for the fluid-droplet interaction and defined by the following formula:

$$Sk = \rho d^2 V_{\mathrm{inlet}}/\mu D \qquad 13$$

where, μ is the dynamic viscosity of the vapor and D is the pipe diameter.

The *Sk* number deals with the interaction between the water droplet and dry solid wall at a temperature of 150 °C. The experimental work conducted by Tran et al., and Liang and Mudawar [29,30] describes the in-depth study of various types of droplet impact on the dry heated solid wall and the diagram of the regimes with the coordinates We number/wall temperature. This regime is specified by Tran et al. [29] and is characterized by a complicated droplet impact. The partial fraction of the droplets is reflected from the wall at t = 2.5 ms and the partial fraction of droplets is evaporated, the reflection feature occurs for an abundance of droplets (t = 1.2–2.5 ms). To describe this impact type, the most suitable approach is to employ the wall-jet boundary condition [30]. This boundary condition is associated with a range of bouncing directions and velocities when a liquid droplet hits a wall. In fact, the wall-jet boundary condition consideration is recommended in hot-droplet wall cases where no liquid film is generated. Conversely, the dominant motion of the droplets is reflection from or sticking to the wall. This feature depends on their wall impact properties. The velocity and direction of the injected particles can be obtained by the subsequent momentum flux, which is a function of the jet impingement angle $\emptyset$ and We number.

Table 2 Relation between Weber number (We) and Stokes (*Sk*) number at Re = 15,000

Re	$d \cdot 10^{-6}$ [m]	*Sk*	*We*	*logWe*
15,000	0.85	0.1	6.8	0.83
	4.7	3	37.6	1.57
	6.1	5	48,8	1.69
	8.1	8	64.8	1.81
	9.0	11	72	1.85
	10.5	15	84	1.92
	12.1	20	96.8	1.99
	15.0	30	120	2.08

Figure 3 shows the various regimes of the droplet impacts. The flow streamlines are depicted in black and the trajectories of the particles are the same color as the particle diameter. The right image represents the movement of the flow and droplets with the velocity magnitude as a background while the left is the magnified view close to the wall. At values of $Sk < 3$, the particle trajectories are close to the flow streamlines and the droplets do not collide with the wall, the particle trajectory only depends on the flow. At $Sk > 20$, the particle trajectory has little dependency on the flow and all the particles travel almost linearly and collide with the wall. In this case, the nature of the particle movement mostly depends on its initial velocity and position. In the range $5 < Sk < 15$, the particle behavior depends on both the initial conditions of the particles and the flow parameters. Notably, the regimes where the droplets do not collide with the wall do not provide high heat transfer from the wall, as the primary heat exchange mechanism here is the evaporation of the drops due to contact with the heated surface. For further calculations in this study, an *Sk* number of 11 is considered suitable to secure a proper heat transfer distribution on the target surface.

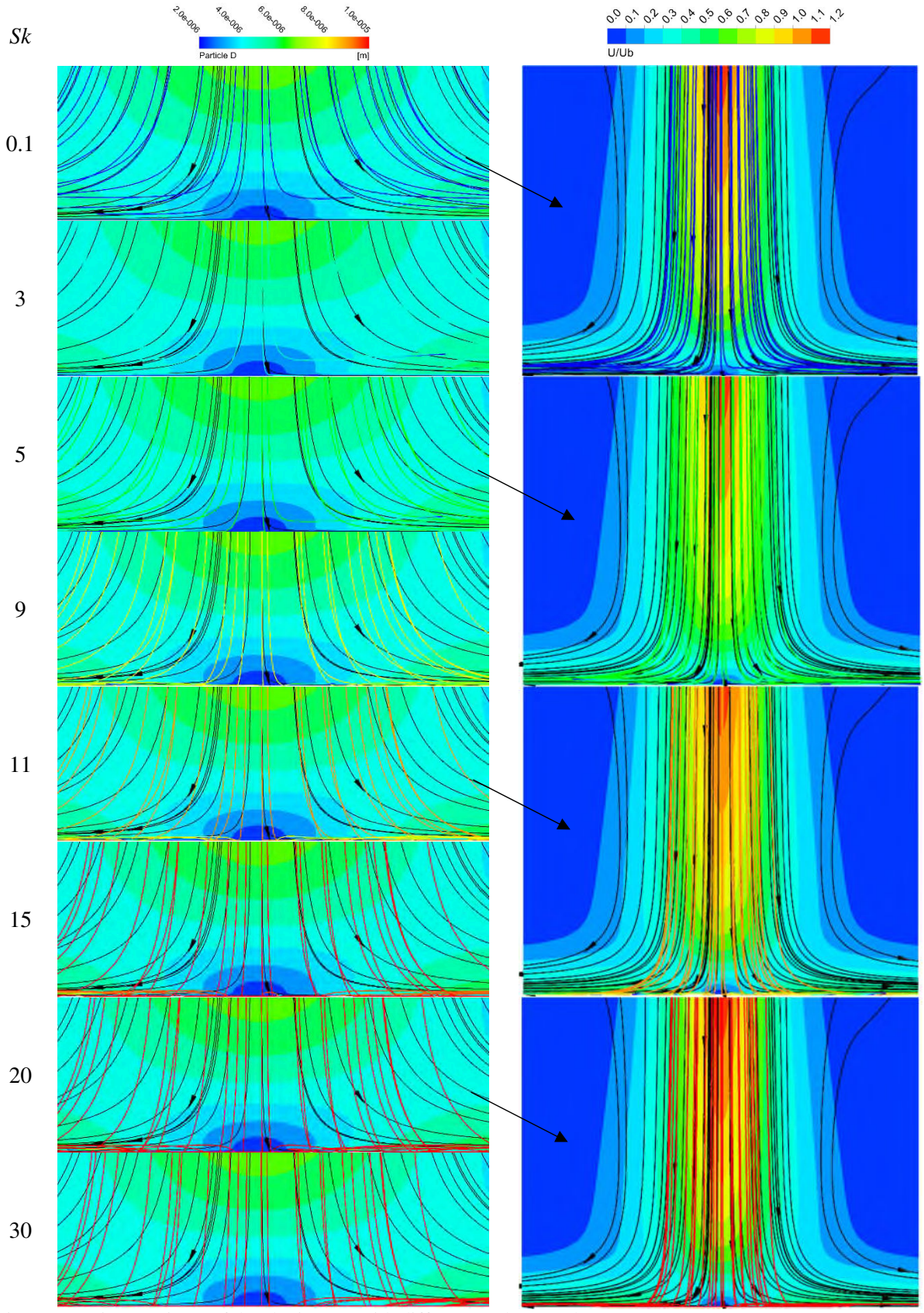

Figure 3 Various regimes of droplet impact with different Stokes number

3.3 Comparison of Mist Injection Technique

In this section, uniform and non-uniform injection scenarios for particle injections are compared and discussed. The uniform injection spreads the particles evenly along the inlet surface area while for non-uniform injection, the particles are injected near the edge of the inlet surface along the curve. The droplet concentration is a function of the distance from the jet center, where the function is considered to be a polynomial equation and is applied to ensure a gradual increase in droplet mass concentration in the free stream near the edge. Furthermore, it guarantees the rapid mass concentration increase near the channel wall until it reaches 85% of the uniform mist concentration as shown in Figure 4 (b) and represented by the dashed line. This distribution is recommended to examine the droplet concentration effects on the heat transfer characteristics.

The particle mass concentration at several distances of y/D is illustrated in Figure 4. As the jet travels towards the target surface, the particles near the edge interact with the surrounding environment. The flow moves towards the target surface as the particles move to the area near the edge away from the jet core. In addition, when the jet reaches y/D = 7, the particle distribution radius increases in size from 0.0067 to 0.0086 m. The results show that the particle injection near the inlet edge is profoundly affected by the surroundings due to the interaction between the jet and its surroundings, which forces the particles to dissipate into the surrounding environment.

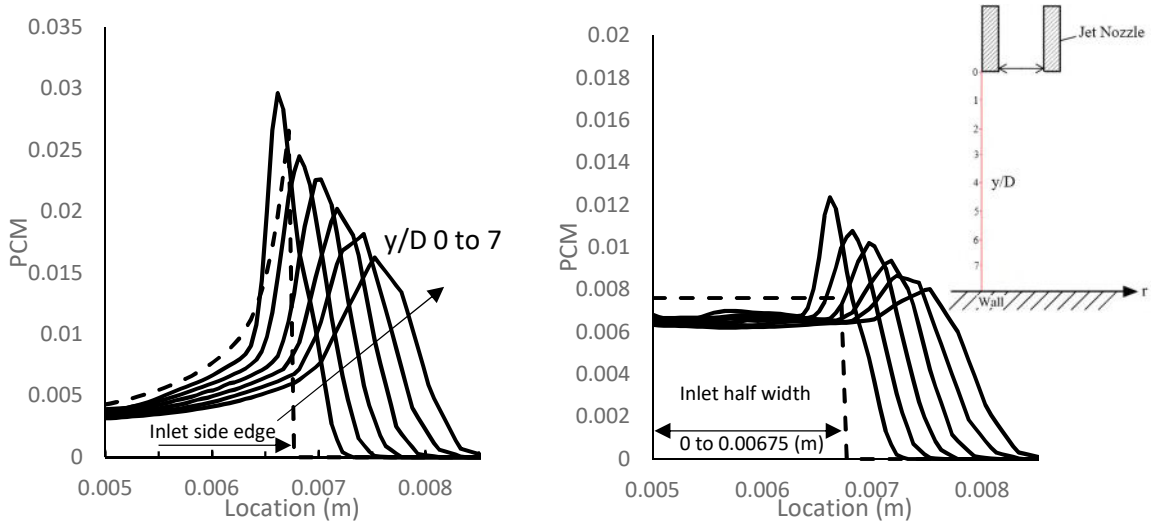

(a) Mist non-uniform distribution (b) Mist uniform distribution

Figure 4 Particle mass concentration at several distances of y/D for different mist distributions; Re = 15,000; mist concentration = 1%

The effect of both uniform and non-uniform injection on heat transfer at different values of H/D and different Re numbers is shown in Figure 5. For all cases, the heat transfer ratio decreases with increasing Re, which is expected as the fluid with high velocity accelerates to escape without absorbing any heat. At different Re numbers, the non-uniform injection technique produces a better heat transfer ratio at different values of H/D (H/D = 2, 4, and 6) compared to the uniform technique. This is

not the case at H/D = 8, where the uniform injection shows a high heat transfer ratio; this may be due to more particles dissipating to the surroundings. In the case of non-uniform injection, with H/D =2, 4, and 6, the average heat transfer rates are increased by approximately 1.8%, 3.5%, and 2.4%, respectively, when compared to the uniform injection technique. In addition, at H/D = 8 and Re = 45,000 the heat transfer ratio decreases significantly compared to the other cases. This feature is due to the long distance the droplet travels before it collides with the heated wall with the presence of a high velocity difference between the jet and the surrounding medium.

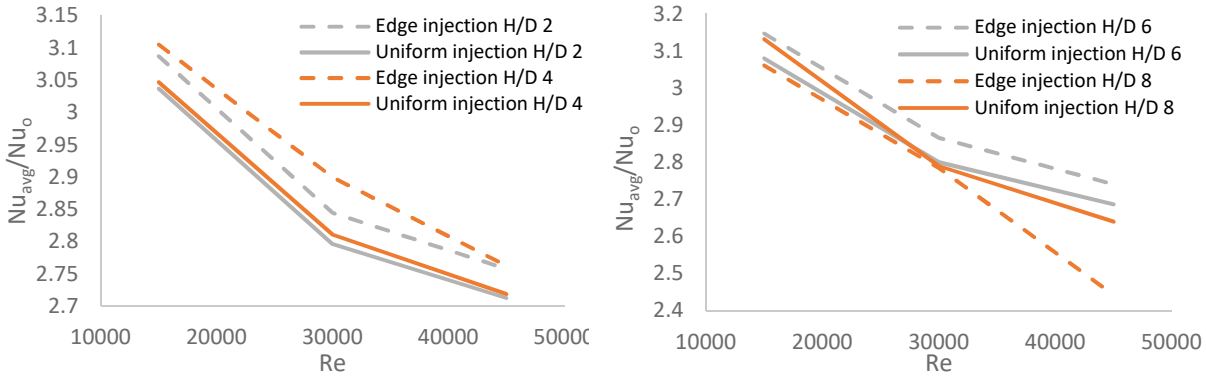

Figure 5 Nusselt number over Dittus-Boelter equation versus Reynolds number at various H/D with different mist distributions

3.4 Effect of Non-Uniform Mist Concentrations on Heat Transfer

Here, the local Nu number is calculated corresponding to cases with a mist concentration of 0% to 4% and with different values of H/D. Figure 6 illustrates the Nu number and particle mass concentration as a function of H/D at Re = 15,000 and a mist concentration of 4%. Particle behavior varies for different values of H/D and the impact diameter increases as H/D increases. Thus, as the free jet develops, it interacts with the surroundings which causes an increase in the width of the free jet diameter and reduces the jet potential core. This prevents particles from hitting the wall directly and causes them to travel for longer in the downstream direction before they actually hit the wall.

Additionally, Figure 6 shows the effects of the particle impact speed on the separation region. In the case where H/D = 2 the particles hit the wall at high speed and, consequently, create a large separation region while at H/D = 8 the separation region is much smaller due to the low impact speed of the particles. At the lower jet to plate distance of H/D = 2, the heat transfer in the collision zone is enhanced. Furthermore, as H/D increases, the particles diffuse through a large area of impact and reduce the heat transfer enhancement in the stagnation region.

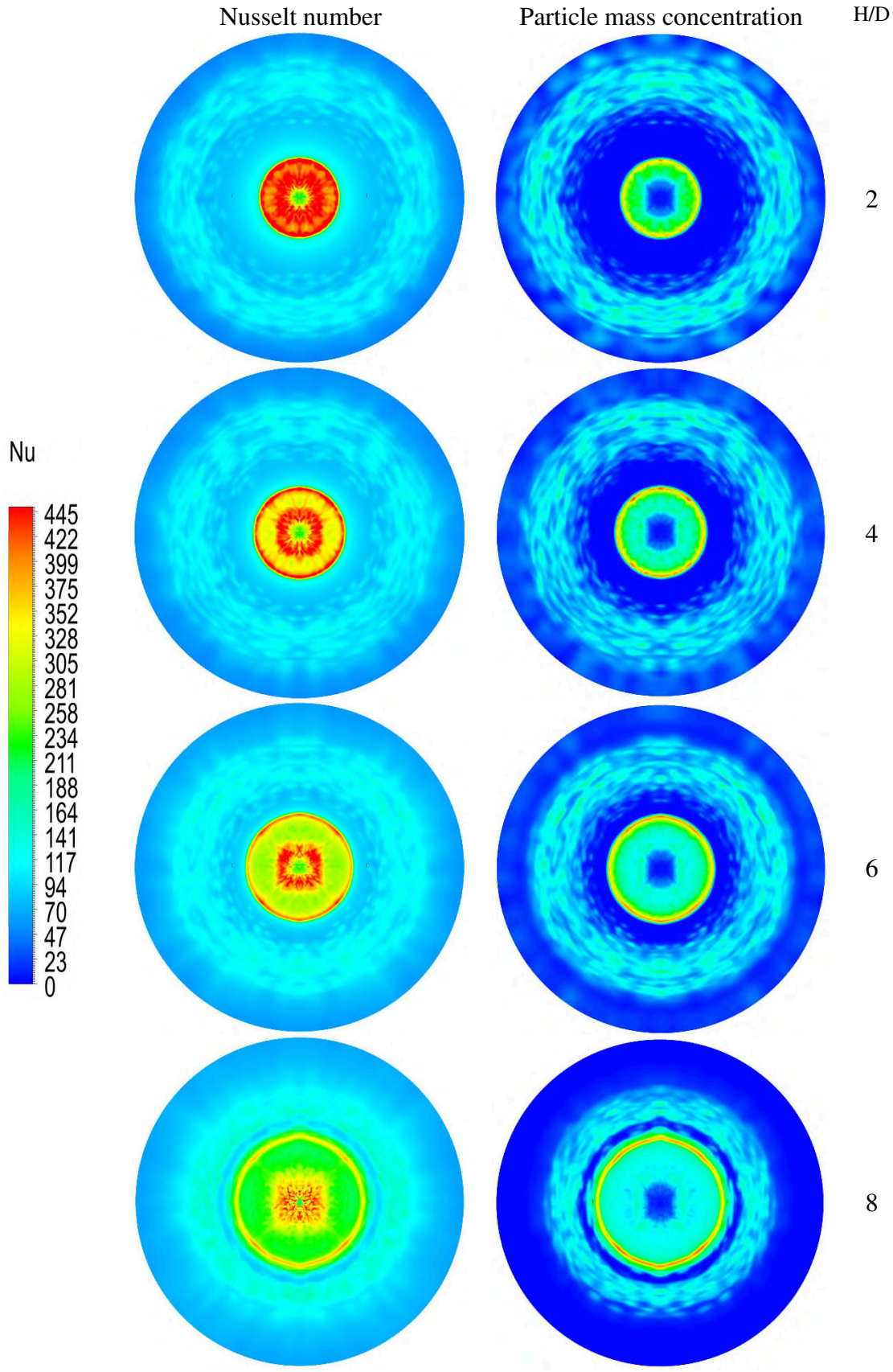

Figure 6 a) Local Nusselt number distribution; b) Particle mass concentration at Re = 15,000 and mist ratio of 4%

Figure 7 shows the local Nu number trend at various r/D and H/D values for mist/steam. At H/D = 2, the heat transfer rate significantly increases once the flow has passed the stagnation point for all mist concentration values due to the number of water particles that collide with the wall in this area, up to r/D = 1.4. This region will be identified as the maximum heat transfer region. In the region of r/D = 0 to 1.4, two peak heat transfer rate values exist for all mist concentrations. Due to the dense mist, the second peak develops close to the first peak, from r/D = 0.74 deviation at low mist ratio to r/D = 0.5 deviation at high mist ratio.

From r/D = 1.4 to 3, a sharp reduction in the heat transfer rate is observed, where the maximum difference of Nu is 3% through this region between all mist fractions. This may be because the particles collided and separated from the wall at H/D = 1.4. This region will be identified as the trough region. After the trough region, a third peak in heat transfer appears, especially at a mist concentration of ≥ 1. This region is identified as the third peak region where the particle reattaches to the wall. After r/D = 4.5, the Nu decreases gradually because the particle size decreases while it combines with the main flow and moves away from the wall and also due to the momentum exchange between the flow and the heated wall.

If the H/D increases, the heat transfer behavior changes, as shown in Figure 7. The maximum heat transfer region expands as H/D increases. Moreover, in this region the distance between the two peaks increases linearly with an increase in H/D due to the nature of the flow. By increasing the H/D value, the free jet diameter increases, which itself drives the particle away from the stagnation region to collide with the wall at a distance. Furthermore, the trough region is maximum at H/D = 2 and decreases with an increase in H/D. The trough region diminishes at H/D = 8 due to the expansion of the maximum heat transfer region and approach to the third peak.

3.5 Maximum and Stagnation Heat Transfer

Figure 8 represents the maximum local heat transfer and stagnation heat transfer at different mist concentrations with various H/D values. The results show that the maximum Nu is achieved at H/D = 2 and the heat transfer decreases for all other cases including the baseline case. Similar observations are reported with the stagnation Nu number correlation developed by Jiang et al. [23]. For most cases, the maximum heat transfer occurs at the stagnation point but when the non-uniform mist is injected into the flow, the maximum heat transfer occurs at a certain radial distance from the stagnation center. Moreover, at H/D = 2, the maximum enhancement occurs with a mist concentration of 4% compared to other mist concentrations. This enhancement increases by 265% compared to the baseline case.

Heat transfer gradually decrease as H/D increases when mist is introduced for H/D = 2, 4, 6. This is due to the mist concertation near the stagnation region as seen in Figure 7. Furthermore, for base case (steam) maximum heat transfer occurs at H/D = 6. This is not the case when mist was injected where lowest heat transfer was found at H/D = 6. This is due to the spread of mist particle near the stagnation point resulting in maximum heat transfer in the stagnation point as shown in Figure 8b. Additionally, at H/D =2, 4 maximum heat transfer increased by 160% and 130% respectively at 2% mist. The same observation was reported by [23] where an increase of heat transfer of ~155% at H/D=3.

The maximum stagnation Nu can be observed at H/D=6 where the minimum stagnation Nu values where spotted at H/D=8 for all tested cases as well. This due to the fact that the stagnation Nu values depend mainly on the trade-off between flow velocity and flow turbulence Just before the jet hits the heated surface. All base case (steam) Nu value at the stagnation point have good agreement with the stagnation Nu correlation obtained by [26].

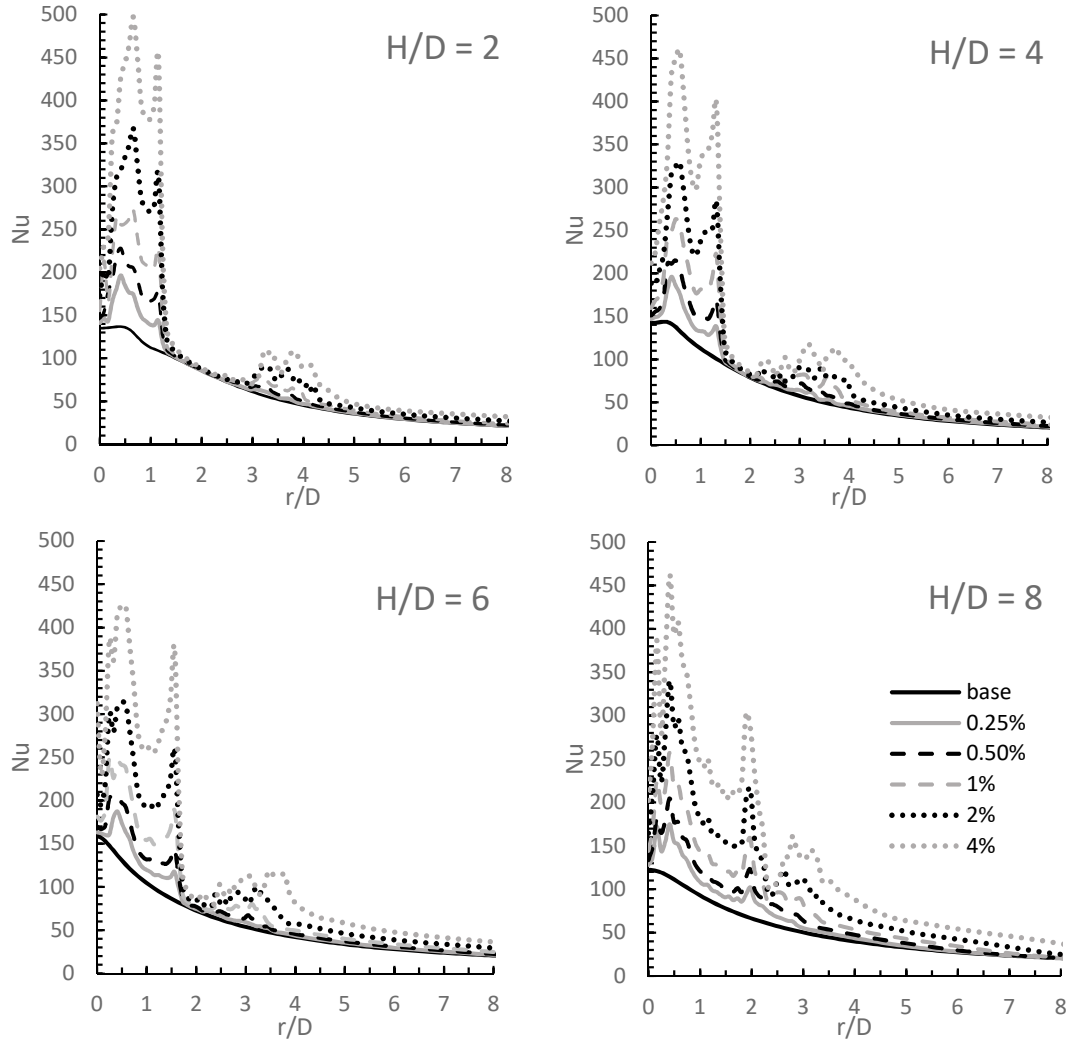

Figure 7 Local Nusselt number at Re = 15,000

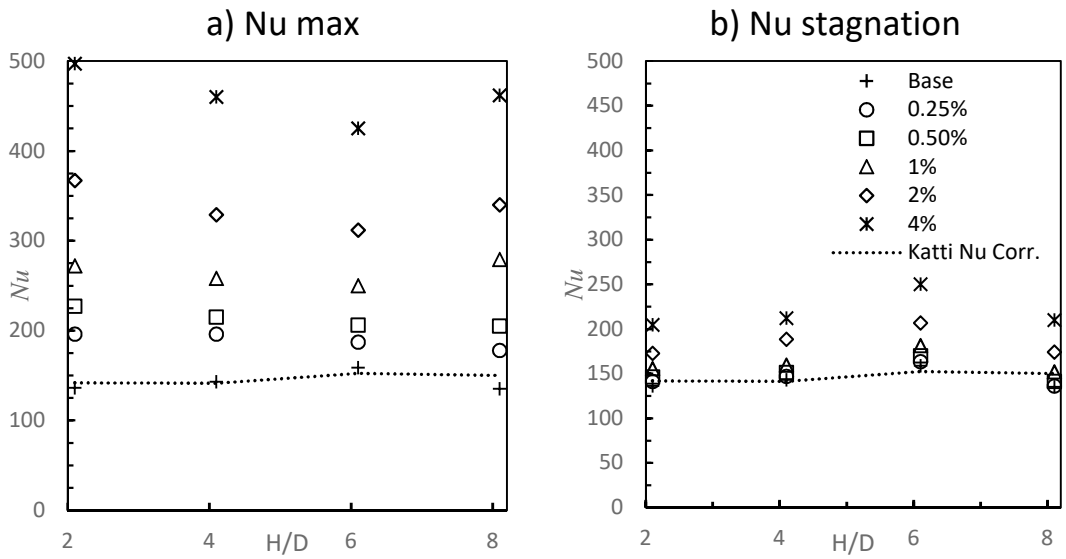

Figure 8 a) Maximum and b) Stagnation local Nusselt number at various H/D for mist ratios 0–4

3.6 Effect of Reynolds number on Wall Averaged Nusselt Number in Mist/Steam

The behavior of the heat transfer enhancement is observed as distinctive for each case. To evaluate the overall enhancement, the wall averaged Nu number is considered at different Re number values. Figure 9 illustrates the wall averaged Nu numbers for two areas with diameters of 2D and 5D over a range of Re numbers to evaluate the enhancement of heat transfer for small and wide targeted areas. At H/D = 2, the averaged Nu over 5D with 4% mist is close to the averaged Nu over 2D for the steam only case. The percentage increase in Nu number is higher for 2D than for 5D because the water particles are more concentrated near the stagnation region. For example, in the case where H/D = 8, the increase in the averaged Nu in the area with a diameter of 2D and 5D is 221% and 151%, respectively, compared to the baseline case.

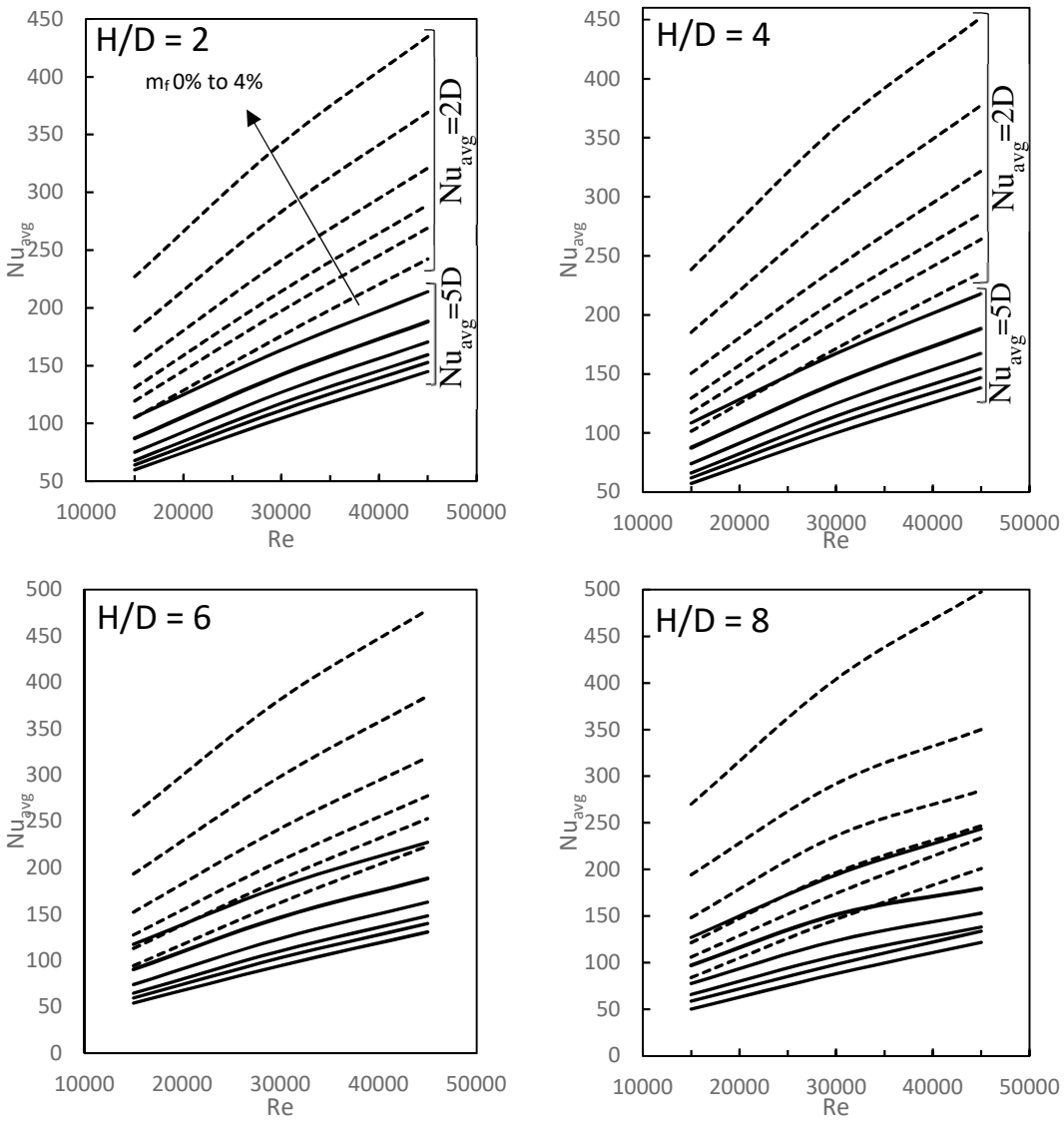

Figure 9 Wall averaged Nusselt number at various Reynolds number values

The ratio of mist averaged Nu to steam only averaged Nu_{base} for unconfined jet impingement is shown in Figure 10. The Nu value decreases as the Re number increases for all values of H/D. The maximum difference occurs at H/D = 8. Besides, the maximum enhancement ratio reaches 3.21 at the same H/D for Re = 15,000 and 4% mist. Furthermore, the result shows that the Re effect increases as the H/D increases, where the Nu decreased by 16% for H/D = 2 and 23% for H/D = 8, and the Re increased from 15,000 to 45,000 for 4% mist.

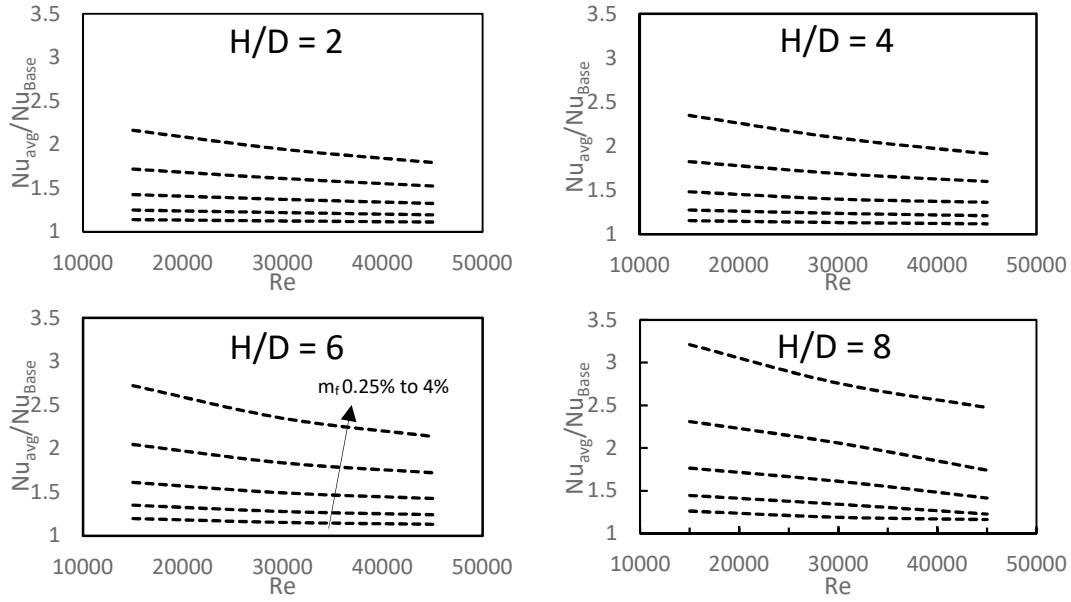

Figure 10 Mist averaged Nusselt number to steam averaged Nusselt number ratio versus various Reynolds number values

4. Conclusion

This study examines the effects of mist addition in the uniform and non-uniform distributions on the heat transfer for unconfined impingement jet flow. The following items can be concluded:

- The droplet stock number has a major impact on droplet behavior. When the *Sk* number is equal to 11, the droplets are fully dependent on the flow behavior and collide with the target wall, while with lower *Sk* numbers most of the particles do not collide with the wall. It can also be mentioned that with higher *Sk* numbers, the droplets are independent of the baseline case flow.
- Non-uniform injection shows higher heat transfer rates at H/D = 2, 4, and 6 than uniform injection but for H/D = 8 uniform injection shows better heat transfer rates for 1% mist.
- The heat transfer characteristic changes significantly by changing the mist injection technique.
- The H/D value has a substantial effect on the droplet behavior interacting with the wall. As the H/D values decrease, the trough region created by the droplet separation and reattachment increase due to the droplet impact speed variation.
- In jet impingement applications, a maximum of two Nu peaks on the heated wall usually exist but when mist is introduced more peaks exist.
- The heat transfer peak pushes farther from the jet stagnation region when the mist is introduced.

Acknowledgments

The authors acknowledge the valuable support and assistance provided by Public Authority for Applied Education and Training (PAAET), in state of Kuwait, through the financial support under project no. TS-19-01.

Nomenclature

D	Nozzle diameter, [m]
d	Droplet diameter, [m]
H	Height between nozzle edge and target wall, [m]
h	Heat transfer coefficient
Nu	Nusselt number, [-]
PCM	Particle mass concentration
Q	Heat flux, [$W \cdot m^{-2}$]
r	Radial distance from stagnation point, [m]
Re	Reynolds number of nozzle, [-]
Sh	Sherwood number, [-]
Sk	Stokes number, [-]
T	Temperature, °C
U	Mass flow average inlet velocity, [$m \cdot s^{-1}$]
We	Weber number, [-]

Greek symbols

λ	Thermal conductivity, [$W \cdot m^{-1} \cdot K^{-1}$]
μ	Viscosity, [$kg \cdot m^{-}1 \cdot s^{-1}$]
ρ	Density, [$kg \cdot m^{-3}$]
σ	Droplet contact angle

Subscripts

avg	Average
base	Steam only
inlet	Nozzle inlet
p	Particles
ref	Reference conditions at nozzle inlet
v	Vapor
wall	Heated wall

References

[1] A. Sexton, J. Punch, J. Stafford, N. Jeffers, The thermal and hydrodynamic behaviour of confined, normally impinging laminar slot jets, Int. J. Heat Mass Transf. 123 (2018) 40–53.

[2] E. Baydar, Y. Ozmen, An experimental investigation on flow structures of confined and unconfined impinging air jets, Heat Mass Transf. 42 (2005) 338.

[3] J.-Y. San, W.-Z. Shiao, Effects of jet plate size and plate spacing on the stagnation Nusselt number for a confined circular air jet impinging on a flat surface, Int. J. Heat Mass Transf. 49 (2006) 3477–3486.

[4] N. Gao, D. Ewing, Investigation of the effect of confinement on the heat transfer to round impinging jets exiting a long pipe, Int. J. Heat Fluid Flow. 27

(2006) 33–41.

[5] D. Lytle, B.. Webb, Air jet impingement heat transfer at low nozzle-plate spacings, Int. J. Heat Mass Transf. 37 (1994) 1687–1697.

[6] D.W. Colucci, R. Viskanta, Effect of nozzle geometry on local convective heat transfer to a confined impinging air jet, Exp. Therm. Fluid Sci. 13 (1996) 71–80.

[7] K.S. Choo, S.J. Kim, Comparison of thermal characteristics of confined and unconfined impinging jets, Int. J. Heat Mass Transf. 53 (2010) 3366–3371.

[8] M.A. Pakhomov, V.I. Terekhov, The effect of confinement on the flow and turbulent heat transfer in a mist impinging jet, Int. J. Heat Mass Transf. 54 (2011) 4266–4274.

[9] J.-Y. San, C.-H. Huang, M.-H. Shu, Impingement cooling of a confined circular air jet, Int. J. Heat Mass Transf. 40 (1997) 1355–1364.

[10] F.N.M. Elwekeel, A.M.M. Abdala, Effect of mist cooling technique on exergy and energy analysis of steam injected gas turbine cycle, Appl. Therm. Eng. 98 (2016) 298–309.

[11] D.I. Rylatt, T.S. O'Donovan, Heat transfer enhancement to a confined impinging synthetic air jet, Appl. Therm. Eng. 51 (2013) 468–475.

[12] S. Pachpute, B. Premachandran, Experimental investigation and large eddy simulations of turbulent slot jet impingement cooling of a circular cylinder with and without a quadrilateral confinement, Appl. Therm. Eng. 144 (2018) 854–876.

[13] D.H. Lee, S.J. Kim, Y.H. Kim, H.J. Park, Heat transfer with fully developed slot jets impinging on confined concave and convex surfaces, Int. J. Heat Mass Transf. 88 (2015) 218–223.

[14] L. Tan, J.-Z. Zhang, H.-S. Xu, Jet impingement on a rib-roughened wall inside semi-confined channel, Int. J. Therm. Sci. 86 (2014) 210–218.

[15] B. Markal, O. Aydin, Experimental investigation of coaxial impinging air jets, Appl. Therm. Eng. 141 (2018) 1120–1130.

[16] F.N.M.M. Elwekeel, A.M.M.M. Abdala, Effects of mist and jet cross-section on heat transfer for a confined air jet impinging on a flat plate, Int. J. Therm. Sci. 108 (2016) 174–184.

[17] Q. Bian, J. Wang, Y. Chen, Q. Wang, M. Zeng, Numerical investigation of mist/air impingement cooling on ribbed blade leading-edge surface, J. Environ. Manage. 203 (2017) 1062–1071.

[18] Y.H. Kim, D.H. Lee, S.H. Han, Investigation of impingement surface geometry effects on heat transfer in a laminar confined impinging slot jet, Int. J. Heat Mass Transf. 115 (2017) 347–353.

[19] C. Quinn, D.B. Murray, T. Persoons, Heat transfer behaviour of a dilute impinging air-water mist jet at low wall temperatures, Int. J. Heat Mass Transf. 111 (2017) 1234–1249.

[20] P. Yu, K. Zhu, T. Sun, N. Yuan, J. Ding, Heat transfer rate and uniformity of mist flow jet impingement for glass tempering, Int. J. Heat Mass Transf. 115 (2017) 368–378.

[21] L.H. Saw, H.M. Poon, H.S. Thiam, Z. Cai, W.T. Chong, N.A. Pambudi, Y.J. King, Novel thermal management system using mist cooling for lithium-ion battery packs, Appl. Energy. 223 (2018) 146–158.

[22] M.A. a. Pakhomov, V.I.I. Terekhov, Enhancement of an impingement heat transfer between turbulent mist jet and flat surface, Int. J. Heat Mass Transf. 53 (2010) 3156–3165.

[23] X. Li, T. Gaddis, T. Wang, J.L. Gaddis, T. Wang, Mist/steam heat transfer in confined slot jet impingement, ASME J. Turbomach. 123 (2001) 161–167.

[24] T. Wang, J.L. Gaddis, X. Li, Mist/steam heat transfer of multiple rows of impinging jets, Int. J. Heat Mass Transf. 48 (2005) 5179–5191.

[25] T. Gao, J. Zeng, J. Li, J. Gong, Numerical prediction on mist/steam cooling in a square ribbed channel at real gas turbine operational conditions, Int. J. Heat Mass Transf. 108 (2017) 1089–1102.

[26] V. Katti, S.V. Prabhu, Experimental study and theoretical analysis of local heat transfer distribution between smooth flat surface and impinging air jet from a circular straight pipe nozzle, Int. J. Heat Mass Transf. 51 (2008) 4480–4495.

[27] N. Gao, H. Sun, D. Ewing, Heat transfer to impinging round jets with triangular tabs, Int. J. Heat Mass Transf. 46 (2003) 2557–2569.

[28] H.M. Hofmann, R. Kaiser, M. Kind, H. Martin, Calculations of Steady and Pulsating Impinging Jets—An Assessment of 13 Widely used Turbulence Models, Numer. Heat Transf. Part B Fundam. 51 (2007) 565–583.

[29] T. Tran, H.J.J. Staat, A. Prosperetti, C. Sun, D. Lohse, Drop Impact on Superheated Surfaces, Phys. Rev. Lett. 108 (2012) 36101.

[30] G. Liang, I. Mudawar, Review of drop impact on heated walls, Int. J. Heat Mass Transf. 106 (2017) 103–126.

[31] Ansys Inc, Ansys Fluent User Guide 18.0., (n.d.).